Micro Cracks Distribution and Power Degradation of Polycrystalline Solar Cells Wafer: Observations Constructed from the Analysis of 4000 Samples

Mahmoud Dhimish

University of Huddersfield, Co-Director of Photovoltaics Laboratory, Huddersfield HD1 3DH, United Kingdom

Abstract—In this paper, the impact of Photovoltaic (PV) micro cracks is assessed through the analysis of 4000 polycrystalline silicon solar cells. The inspection of the cracks has been carried out using an electron microscopy, which facilitate the detection of the cracks though the acquisition of both Everhart-Thornley Detector (ETD) and the Back Scatted Electron Diffraction (BSED) image, where it was found that the size micro cracks are ranging from 50µm to a maximum of 4mm. Micro cracks have been categorized into two main categories, including cracks in the solar cell front or rear contact. Several remarkable observations have been found, including but not limited to, (i) the output power loss due to micro cracks varies from 0.9% to 42.8%, subject to micro crack type and size, (ii) cracks in solar cells fingers reduce the finger width, resulting an increase in the output power loss by at least 1.7%, and (iii) there is a substantial correlation between PV hot-spots and the presence of micro cracks, while minimum increase in the cell temperature is observed at 7.6 °C.

Keywords—Photovoltaic Micro Cracks; PV Defects; Hot-Spots; Output Power Loss; Micro Analysis; Electron Microscopy Imaging.

I. Introduction

Nowadays the lifetime of photovoltaic (PV) modules is an important target for the sustainable development of PV technologies. According to the International Electro-Technical Commission (IEC) 61215 PV qualification standard [1], PV modules are subject to multiple failure modes, ultimately an increase of PV micro cracks [2-3] and PV hot-spotting phenomenon [4-5] have been widely acknowledged. For instance, limited approaches and examination of such faults have been raised, and therefore, further data inspection and validation of typical PV failure have to be assessed and analysed comprehensively.

In order to examine PV micro cracks several methods have been proposed, including but not limited to the Laser scanning technique [6], Electron Microscopy (EM) analysis [7], Photoluminescence (PL) imaging technique [8], and the widely used Electroluminescence (EL) method [9].

F. Haase et al. [10] found that PV micro cracks do not reduce the output power of affected solar cells by more than 2.5%, only if the crack does not harm the fingers or busbars. While, a real-time long-term data analysis of multiple cracked PV modules were analysed by M. Dhimish et al. [11]. It was observed that output power of cracked PV modules ranging from -0.5% to -19.7%; depending on the crack size, orientation and location.

35 Furthermore, the micro crack analysis on gallium arsenide (GaAs) PV solar cells has been carried out by S.
36 Oh et al. [12]. It was observed that the crack density, defined as the total length of the micro crack per unit
37 area, is found to be in the range from 13.8 to 33.2 cm-1 in all investigated solar cell samples of 1620. On
38 the other hand, the analysis of the output power loss and cracks distribution have not been considered.

39 PV micro cracks are major cause of hot-spotting. PV hot-spots are a reliability problem in PV modules; this
40 phenomenon is distinguished when a mismatched/cracked solar cell heats up significantly and reduces the
41 PV module output power [13-14]. PV hot-spots can be easily detected using infrared inspection, which
42 nowadays has become a common practice in current PV fault diagnosis as presented in [15]. However, the
43 correlation between micro cracks and hot-spotting has not widely been considered, while the largest up-to-
44 date study on PV hot-spotting has been reported by our previous work [16]. Furthermore, PV hot-spots can
45 cause a permanent loss in the output power of PV module, and could be reach up to -25% of the PV module
46 maximum power point.

47 PV hot-spotting can be mitigated using various methods such as novel distributive maximum power point
48 tracking (MPPT) method [17-18], adoption of bypass diodes which are parallelized with the PV modules
49 [19], and most recently, a novel two MOSFET layer method developed by [20-21] improved the output
50 power of hot-spotted PV modules by at least 8% under various environmental conditions.

51 The main contribution of this work is to present the impact of micro cracks; ranging from 50µm to a maximum
52 of 4mm, on the output power performance of solar cells. A total of 4000 cracked samples has been examined.
53 Various major findings have been observed, including:

54   1) The output power loss due to micro cracks ranging from 0.9 to 42.8%.
55   2) Cracks in solar cells fingers reduce the finger width, resulting an increase in the power loss.
56   3) There is a substantial correlation between the hot-spots and micro cracks, multiple results were observed
57   by the reason of the heat expansion due to the micro cracks affect.

II. Methodology
A. Electron Microscopy

60 Nowadays in order to examine the micro cracks in the solar wafers, an electron microscopy shown in Fig.
61 1 has been used. The microscopy is interfaced with a personal computer (PC) using a data acquisition board.
62 The acquisition of both the Everhart-Thornley Detector (ETD) and the Back Scatted Electron Diffraction
63 (BSED) is facilitated using the acquisition board as presented Fig. 1.

64 The BSED is a microstructural-crystallographic characterization technique normally use to study any
65 crystalline or polycrystalline materials [22], whereas the ETD consists of a secondary electron and back-
66 scatted electron detector, this detector is used to increase the efficiency of existing secondary electron
67 detectors by adding a light pipe to carry the photon signal from the scintillator inside the evacuated
68 specimen chamber of the electron microscopy [23]. In fact, it is not necessary to capture both images, but,
69 for a better resolution and detection of the inspected wafer, both images have been captured.
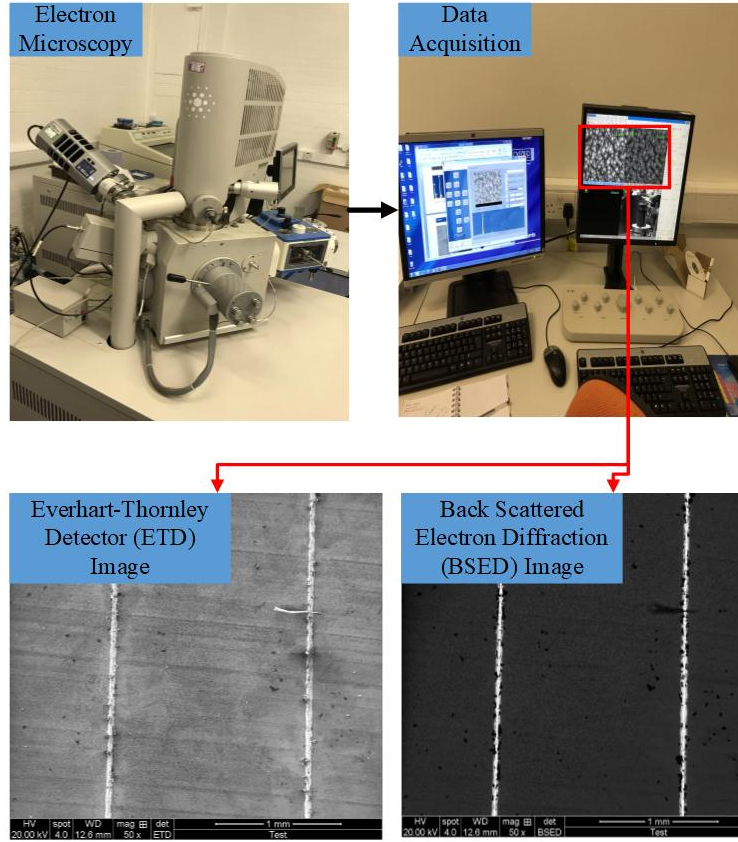
Fig. 1. Electron microscopy facility used to inspect the cracked solar cell samples. The microscope has a data acquisition system which facilitate the monitoring for both the ETD and BSED images using a personal computer

B. Examined Solar Cell Samples

In this article, the examination of 4000 cracked solar cell have been examined; example of multiple samples are shown in Fig. 2(a); showing both front and rear view for diffident types of cracks. All tested samples are dismounted from actual PV modules operated in a field across the UK. The solar cells have been on actual operation for 5 to 13 years.

All main electrical parameters of the cracked samples have been tested under standard test conditions (STC), where the solar irradiance is equal to 1000 W/m2 and ambient temperature of 25 ℃; main electrical parameters are shown in Table 1.

Fig. 2(b) shows the location of the fingers and the solar cell busbar. Solar cell fingers are the metallic rectangular–shape grid connecters which collect the generated current for devilry to the busbar. The busbar is constructed from copper, coated with silver to enhance the current conductivity (front side) as well as to lower oxidization (rear side).

Table 1 Examined solar cells main electrical parameters

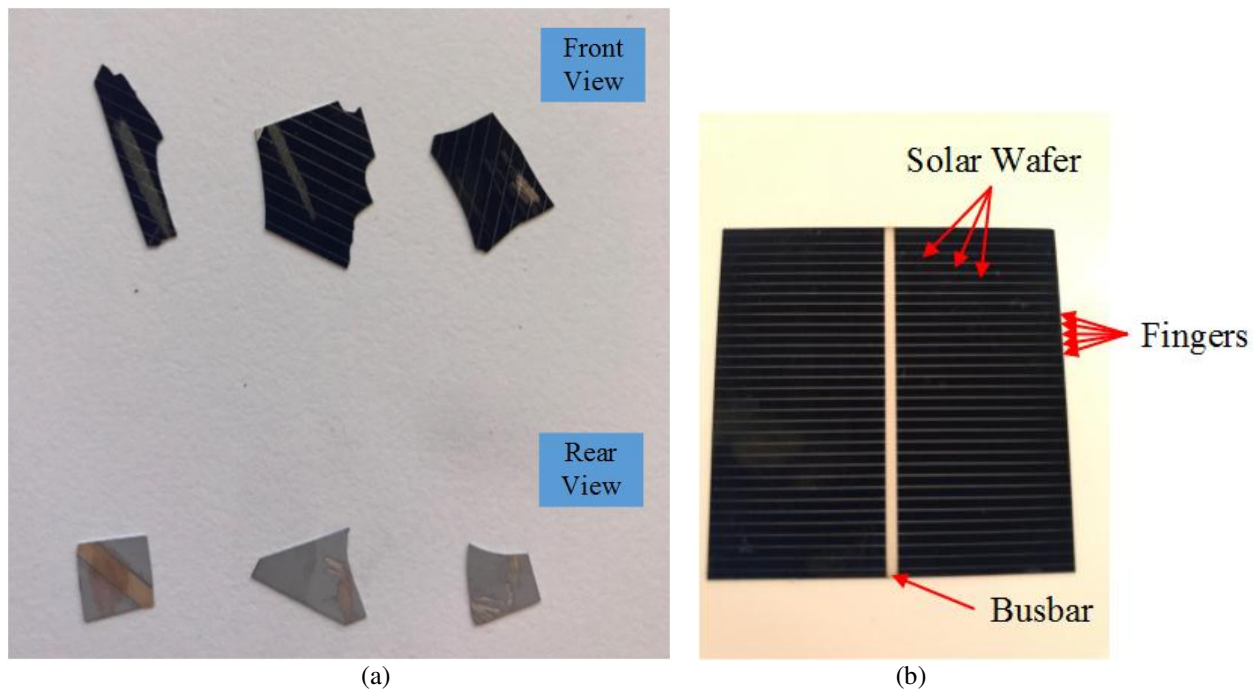| Electrical Parameter	Theoretical Value – Taken form manufacturer data sheet
Voltage at maximum power point (V_{mpp})	0.48 V
Open circuit voltage (V_{oc})	0.61 V
Power at maximum power point (P_{mpp})	3.10 W
Current at maximum power point (I_{mpp})	6.46 A
Short circuit current (I_{sc})	7.12 A

Fig. 2. (a) Example of the front and rear view for multiple examined solar cell wafers, (b) Solar cell wafer, fingers and busbar

C. Distribution and Data Collection Process

The examined solar cells samples have been distributed according to the existence of the micro crack type. The analysis and data collection were distributed across front and rear view/side of the solar cell damage, including:

Front View:

1) Wafer + Fingers (Fig. 3(a)): micro cracks affecting both wafer and the fingers of the solar cell.
2) Wafer + Busbar (Fig. 3(b)): existence of micro cracks on solar cell wafer and busbar, but not fingers.
3) Wafer + Fingers + Busbar (Fig. 3(c)): micro cracks affecting the wafer, fingers, and the busbars.

Rear Contact:

1) Micro cracks affecting rear surface of the solar cell, example shown in Fig. 3(d).
2) Micro cracks affecting both rear surface of the solar cell and the rear busbar, example shown in Fig. 3(e).

All observed micro cracks have a length ranging from 50µm to a maximum of 4mm, therefore, the output power analysis as well as the observations in the rest of the article are based on this assumption, and ultimately, different crack length would result different observations.

The percentage of occurrence of the micro cracks in all tested samples are summarized as follows:

1) Wafer + Fingers presenting 39%; 1560 samples.
2) Wafer + Busbar presenting 17%; 680 samples.
3) Wafer + Fingers + Busbar presenting 36%; 1440 samples.
4) Rear surface presenting 6%; 240 samples.
5) Rear surface + Rear Busbar presenting 2%; 80 samples.

4

104   It is worth noting that the number of cracked busbars or fingers has not been considered in the data analysis.
105   There are two reasons behind this choice including, **(i)** the data collection and analysis of the output power
106   loss will fluctuate rapidly if the number of fingers and busbars are counted, and **(ii)** in order to draw relevant
107   conclusions with the consideration of multiple case studies, it would help to classify which micro crack
108   type/category has the most significant impact on the output power loss; resulting a generic/extensive gained
109   knowledge on the studied samples, where the outcomes can be used extensively across a number of other
110   studies, including PV degradation, PV manufacturing analysis and solar cell micro cracks detection
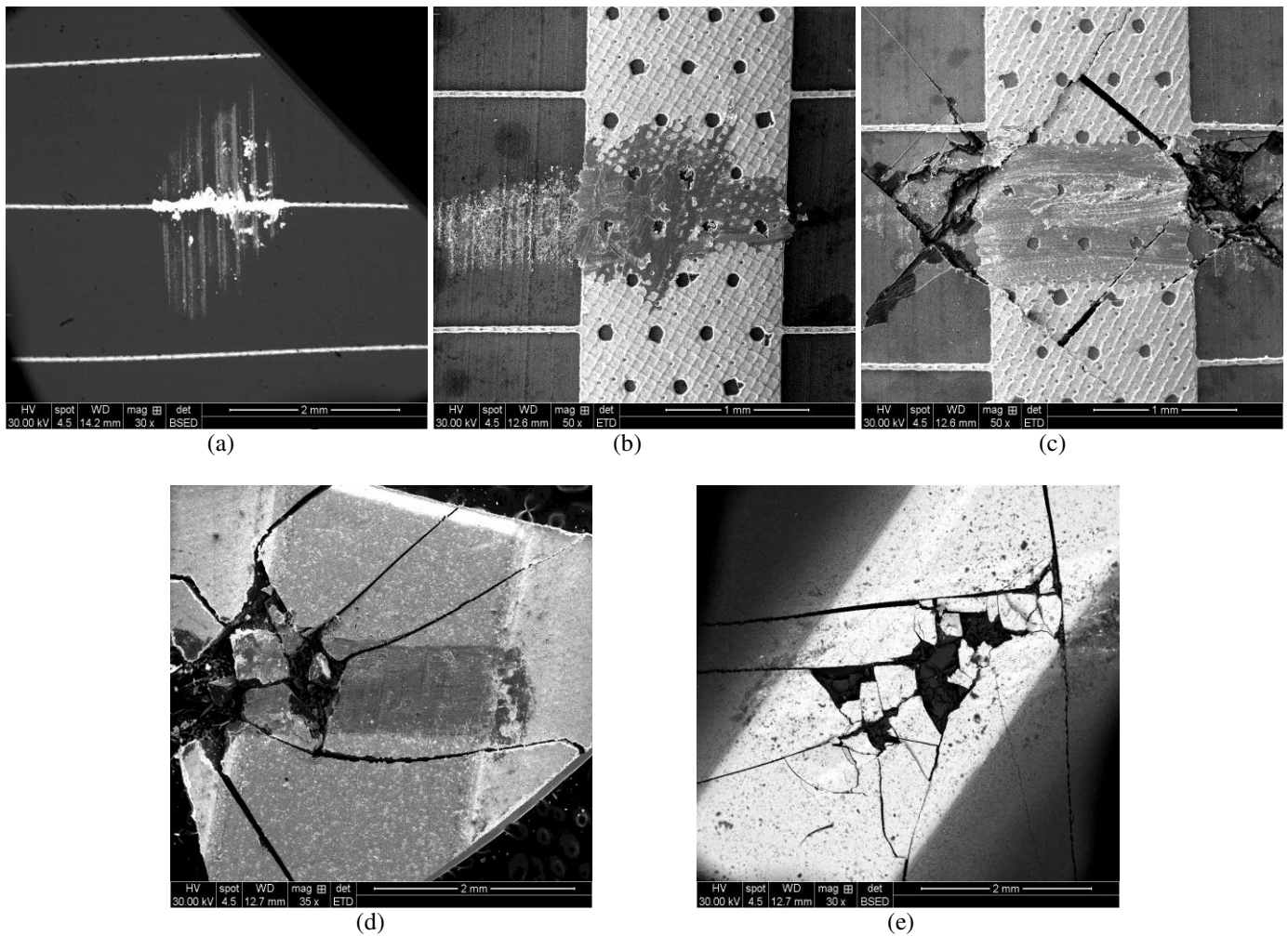111   systems.

Fig. 3. Examples of the distribution for the micro cracks in different solar cell samples. (a) Micro cracks affecting solar cell wafer and fingers, (b) Micro cracks affecting solar cell wafer and busbars, (c) Micro cracks affecting solar cell wafer, fingers and busbar, (d) Micro cracks in the rear surface of the solar cell, (e) Micro cracks affecting rear surface of the solar cell as well as the rear busbar

III.   Results
A. Power Loss Analysis

In this section, the evaluation of the power loss of all examined PV solar cell is presented. The measured power loss of the solar cells is captured while experimentally illuminating the cells under standard test conditions (STC), where the solar irradiance is equal to 1000 W/m^2, and cell surface temperature of 25 °C, the experimental setup is shown in Fig. 6(b). The output power loss is measured by the following formula:

$$Power\ Loss\ (\%) = 100 - \left(\frac{P_{Micro\ cracked\ solar\ cell}}{P_{Theoretical\ maximum\ power}} \times 100\right) \qquad (1)$$

where $P_{Micro\ cracked\ solar\ cell}$ is the actual measured output power of the tested micro cracked solar cell sample, whereas $P_{Theoretical\ maximum\ power}$ is the theoretical power taken from the datasheet; the value for the theoretical power is equal to 3.1 W, presented earlier in Table 1.

According to Fig. 4(a), the solar cell samples affected by cracks in the front contact have a power loss ranging from:

    1) Cracks in Wafer + Finger: -1.7% to -13.5%.
    2) Cracks in Wafer + Busbar: -0.9% to -17.1%.
    3) Cracks in Wafer + Finger + Busbar: -8.9% to -42.8%.

Evidently, the cracks affecting solar wafer, fingers and the busbar have the uppermost power loss, with mean of 25.52%, whereas the second maximum mean output power loss of 9.01% is obtained for the solar cells affected by micro cracks in the solar wafer and the busbar. The minimum output power loss is observed for solar cells that are affected by micro cracks across the wafer and fingers, their mean output power loss is equal to 7.59%.

According to the solar cell samples affected by rear contact micro cracks, it was observed that loss in the output power is very limited (mean of 1.48%) for the rear surface cracks, however, there are an increase in the output power loss due to the rear contact cracks affecting both surface and the rear busbar, where it was found that the mean output power loss is equal to 7.99%.

It is noticeable that front contact micro cracks have the most significant impact on the overall performance of the solar cells because these cracks affects the surface of the junction, ultimately limiting the amount of solar energy to be extracted by the cell. On the other hand, the output power loss for micro cracked rear surface is far less than the front contact, since it is much further away from the junction, whereas the rear busbar plays significant role in driving the solar cell current, therefore, cracks in rear and front busbar have a much higher output power loss.

There are a number of observations that have been identified using the studied sample set, including the correlation between micro cracks and hot-spots in the micro cracked solar cells. These observations are discussed in the following sections.
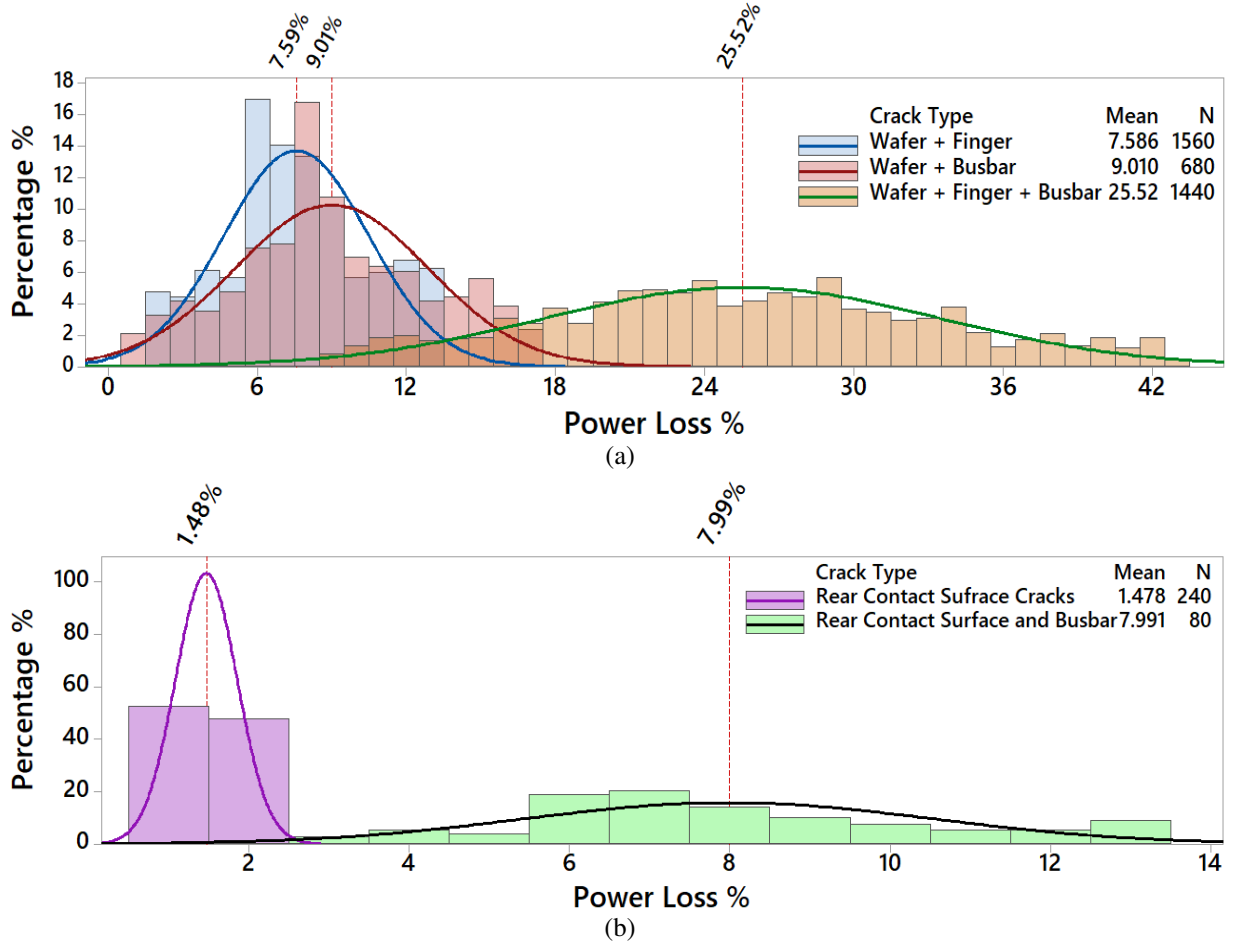
Fig. 4. Power loss analysis of the cracked solar cell samples. (a) Front contact crack-types, (b) Rear contact crack-types

B. Effect of Breakdown/Micro-Cracks in Solar Cells Fingers

Due to the existence of micro cracks, it was observed that out of all examined samples, almost there are 1500 samples that has a breakdown/cracks in the solar cell fingers, resulting a less forward current generation of the solar cell. Two examples of the micro crack, damage and discontinuity in the solar cell fingers are shown in Figs. 5(a) and 5(b).

There is an increase in the output power loss due to the cracked/damaged fingers. In order to calculate the power loss in a single finger, the integration of the length for the finger starting from 0 to L (shown in Fig. 5(c)) gives the power loss as calculated by (2).

$$Power\ loss = \int_{x=0}^{x=L} \frac{(xJ_{MPP}S_f)^2}{w_f\,d_f}d_x = \frac{1}{3}\,L^3\,J_{MPP}^2\,S_f^2\,\frac{\rho_f}{w_f\,d_f} \qquad (2)$$

where $L = 2cm$ is the finger length, $J_{MPP} = 30\ mA/cm^2$ is the current at maximum power point, $S_f = 2mm$ is the finger spacing, $\rho_f = 1.82 \times 10^{-8}\ \Omega m$ is the effective resistivity of the metal, $w_f = 25\ \mu m$ is the finger width, and $d_f = 13\ \mu m$ corresponds to the finger depth (or height); all parameters values are taken from solar cell manufacturer datasheet.
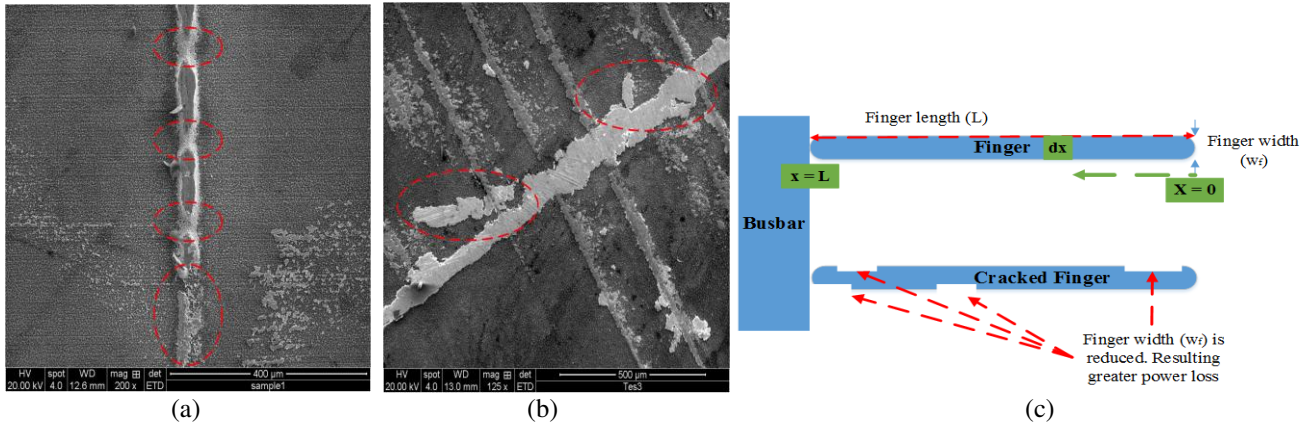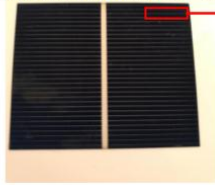
Fig. 5. (a) Cracked – non discontinuity in solar cell finger, sample 1, (b) Cracked – non discontinuity in solar cell finger, sample 2, (c) Illustration on the fingers main parameters, where the width of the cracked finger is reduced resulting a greater power loss

158   As shown in Figs. 7(a) and 7(b), the measured total power loss for the solar cell finger without the existence
159   of micro cracks is equal to 3.8%, while it is increased to 5.0% for the cracked finger sample. The main
160   reason in the increase of the power loss is due to the decrease in the finger width. Therefore, According to
161   (2), if the width of the finger w_f decrease, the finger power loss will increase. Furthermore, the cracks in
162   the solar cell fingers increase the heat-level of the affected solar cell, because the forward current will be
163   delivered though marginal size of metal (due to the reduction of the finger width size). Consequently, this
164   will create a hot-spot in the finger and will reduce the forward current delivered by the cracked cell. Fig.
165   6(a) shows a cracked solar cell sample tested under STC conditions, where two fingers are cracked.
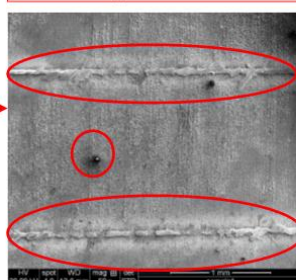
166   The obtained results shown in Fig. 7 are measured using the analysis of a healthy vs. micro cracked solar
167   cell sample under STC. The setup of the class AAA LED flasher is shown in Fig. 6(b). The solar cell sample
168   has been placed inside the LED-based flasher, whereas a control unit is used to attain a light intensity of
169   1000 W/m2 and ambient temperatures of 25 °C. Thereafter, the output power, current and resistive loss are
170   measured using a data acquisition system which uses LabVIEW software. It is also worth noting that all
171   tested samples get an illumination of 1000 W/m2 for a period of 5 milliseconds, this is the fastest rate of
172   change that is possible for the flasher to switch its mode from the on/off state. Therefore the observed heat-
173   map and thermal-image corresponds to the actual change of the heat across the surface of the solar cell.

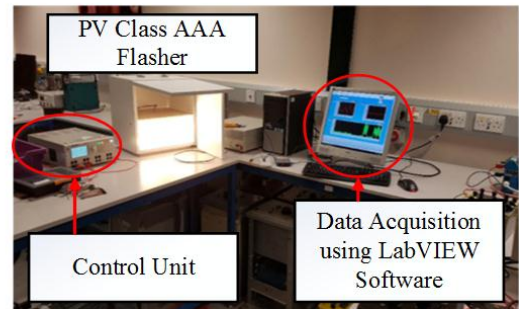Fig. 6. (a) Cracked solar cell tested under STC, (b) PV Class AAA Flasher setup
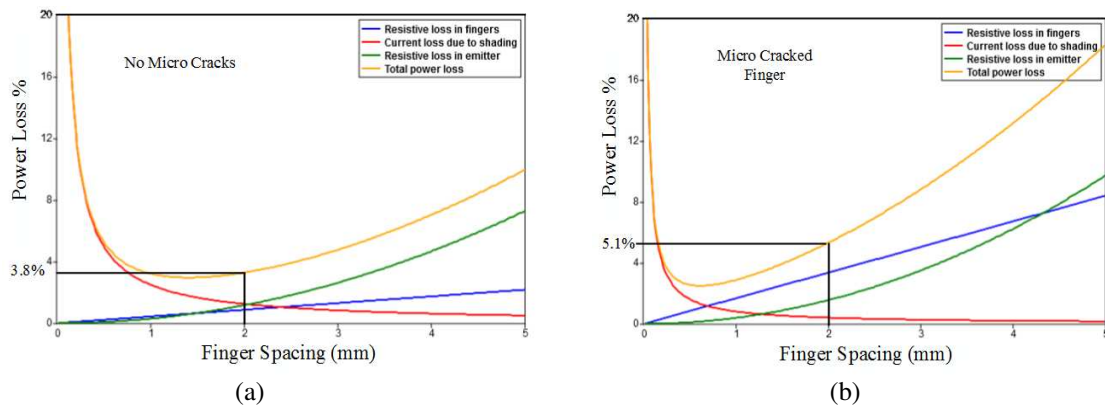
8

Fig. 7. (a) Power loss estimation (~3.8%) for finger without existence of micro cracks, (b) Power loss estimation (~ 42%) for finger including micro cracks

The output heat-map/thermal-image of the solar cell is shown in Fig. 8. By contrast with the results shown in Fig. 8(a), after ten seconds of evaluating the solar cell sample under STC, the temperature of the cracked area raised to 72.6 °C, whereas adjacent regions started to heat-up to a limit of 42.5 °C. Interestingly, due to the expansion of the heat over the whole solar cell, the heat of the cracked area started to decrease due to the flow of the heat over the full cell sample. In Fig. 8(b), thermal image of the solar cell sample is captured after 60 seconds, it is evident that the cracked area has a lower temperature of 43.9 °C, but more area of the solar cell is affected by a rise in the temperature. In addition, according to Fig. 8(c), after 120 seconds (the test sample was still under STC), the solar cell sample almost have an identical temperature level of 34.3 °C, compared to original temperature of 26.7 °C, therefore, the increase of the solar cell temperature due to the existence of the micro cracks is raised by 7.6 °C. It is worth noting that this temperature level remains same after 120 seconds. This result confirms that micro cracks in solar cells cause hot-spots, where the main heat source of the cell is spread from the original cracked area, and it heats up significantly due to the excitation of the electrons through a thinner width of the metal carrying the current either in the fingers or busbars, subsequently an increase in the solar cell temperature will be garneted, as well as an increase in the output power loss would highly be expected.

By contrast with above results, the heat is transferred from the hot-spot area to the rest of the solar cell due to the concept of heat by conduction. Conduction is the transfer of heat energy through a solid by the collision and vibration of molecules in the solar cell, without movement of the bulk material. For example, the hot-spotted area molecules interact with neighboring molecules, transferring some of their energy (heat) to these adjacent particles. And since this heat would decrease in the hot-spotted area and increase in the adjacent area, the solar cell temperature went steady. This phenomenon is well-known by the transient conduction where the heat is not only transferred through the solid using the vibration of the molecules but also as a function of time [24].
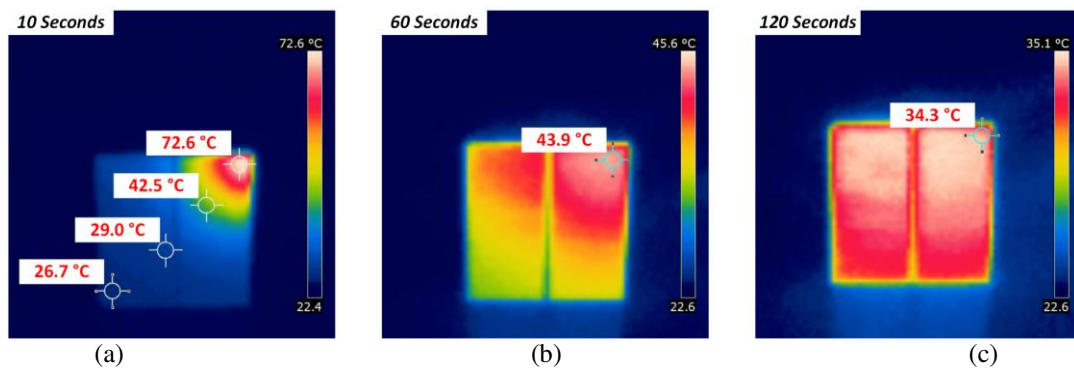

Fig. 8. Heat-Map distribution of the cracked solar cell shown in Fig. 6, operating under STC, images are captured using FLIR thermal camera. (a) After 10 seconds, (b) After 60 seconds, (c) After 120 seconds – this level of temperature remains steady

9

197 According to [25] it was observed that 78% of the reverse power is turned into heat at the hot-spot area.
198 The remaining fraction of the power was evenly distributed over the cell, accounting for the normal reverse
199 current, possible contact resistance and additional small shunts. Consequently, the distribution of the heat
200 over the cell is generated due to the reverse current flowing from the hot-spotted area throughout the cell
201 using the adjacent fingers and busbar, successively reducing the output generated power of the affected
202 solar cell. Similarly, authors in [26] presented a new method which provides simple and fast evaluation of
203 the hot-spotted solar cells. It was shown that the heat of the affected solar cell by possible hot-spots could
204 be distributed across the adjacent locations after a period of 60ms, where the main cause of the heat
205 distribution is due to the existence of non-cracked fingers and busbars.

206 In order to determine the I-V and P-V curves of the solar cell sample under STC, an experiment has been
207 carried out using the class AAA LED flasher shown in Fig. 6(b). The obtained I-V and P-V curves are
208 presented in Fig. 9. Compared to the theoretical predictions (discussed earlier in Table 1), the solar cell
209 sample has almost equal V_{mpp} of 0.48V. However, there is drop in the I_{mpp} by 0.286A; I_{mpp} (theoretical:
210 6.46A) – I_{mpp} (cracked solar cell: 6.174A). Resulting an output power loss of 4.39%; calculated as follows:

211
$$Power\ Loss\ (\%) = \ 100 - \left(\frac{2.964\ (P_{Micro\ cracked\ solar\ cell})}{3.1\ (P_{Theoretical\ maximum\ power})} \times 100\right) = \ 4.39\%$$
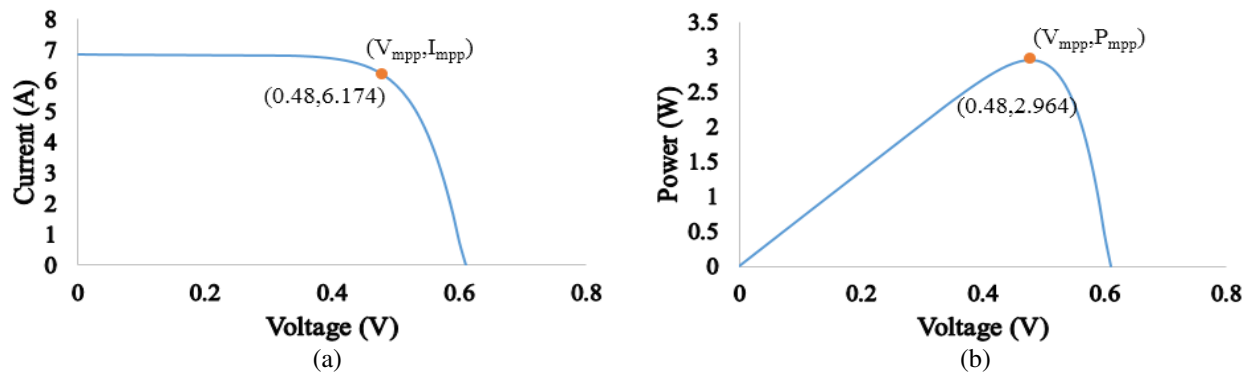

Fig. 9 Obtained I-V & P-V curves of the cracked solar cell sample shown in Fig. 6(a) under STC

212 Another example of cracked fingers has been examined, the cracked cell is shown in Fig. 10. The cell is
213 affected by three cracked fingers, where it is evident that there is a discontinuity in the finger connections,
214 this would result an increase in the amount of heat generated by this particular case.
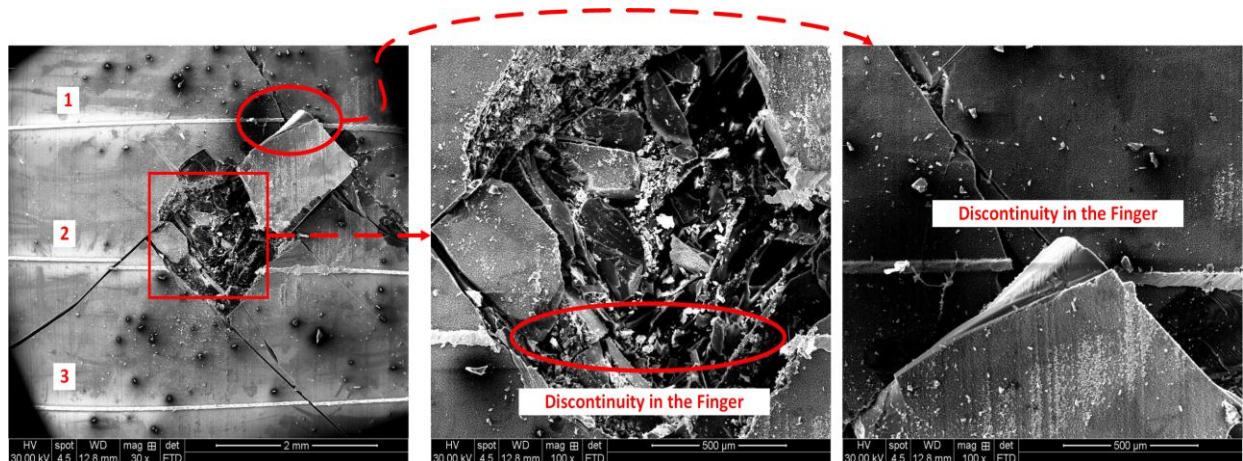

Fig. 10. Micro crack affecting three fingers – there is a discontinuity in the finger connection to the main busbar

215 The examination of the heat-level of the solar cell, starting at 0 second; where the cell has not yet been
216 tested under STC, ending up with 100 seconds, where at this stage the cell temperature remains at constant
217 level. The results of the experiment are shown in Fig. 11.

218 At zero seconds, the temperature of the cell is equal to 24.3 °C. The temperature of the cracked area raised
219 to 105.1 °C after 20 seconds of testing the cell under STC. Ultimately, the heat-level of the cracked would
220 decrease, due to the expansion of the heat over the cell, resulting a temperature levels of:

221   1) 83.6 °C (40 seconds)
222   2) 70.9 °C (60 seconds)
223   3) 55.8 °C (80 seconds)
224   4) 40.2 °C (100 seconds) - this level of temperature remains consistent

225 In contrast with the results of the heat-distribution, the solar cell had an increase in the temperature of about
226 15.9 °C; final temperature level 40.2 °C – original temperature level 24.3 °C. Therefore, this results
227 confirms that micro cracks in solar cells are one of the main cause of PV hot-spotting, as well as, the
228 increase in the size of cracked area, ultimately will increase the heat-level of the hot-spot in the affected
229 solar cell.

230 The solar cell sample has been tested under STC. The obtained I-V and P-V curves are presented in Fig.
231 12. Compared to the theoretical predictions (discussed earlier in Table 1), the sample has almost equal V_{mpp}
232 of 0.47V. However, there is drop in the I_{mpp} by 0.662A. Hence, the output power loss is equal to 12.09%;
233 calculated as follows:

234
$$Power\ Loss\ (\%) = 100 - \left(\frac{2.725\ (P_{Micro\ cracked\ solar\ cell})}{3.1\ (P_{Theoretical\ maximum\ power})} \times 100 \right) = 12.09\%$$
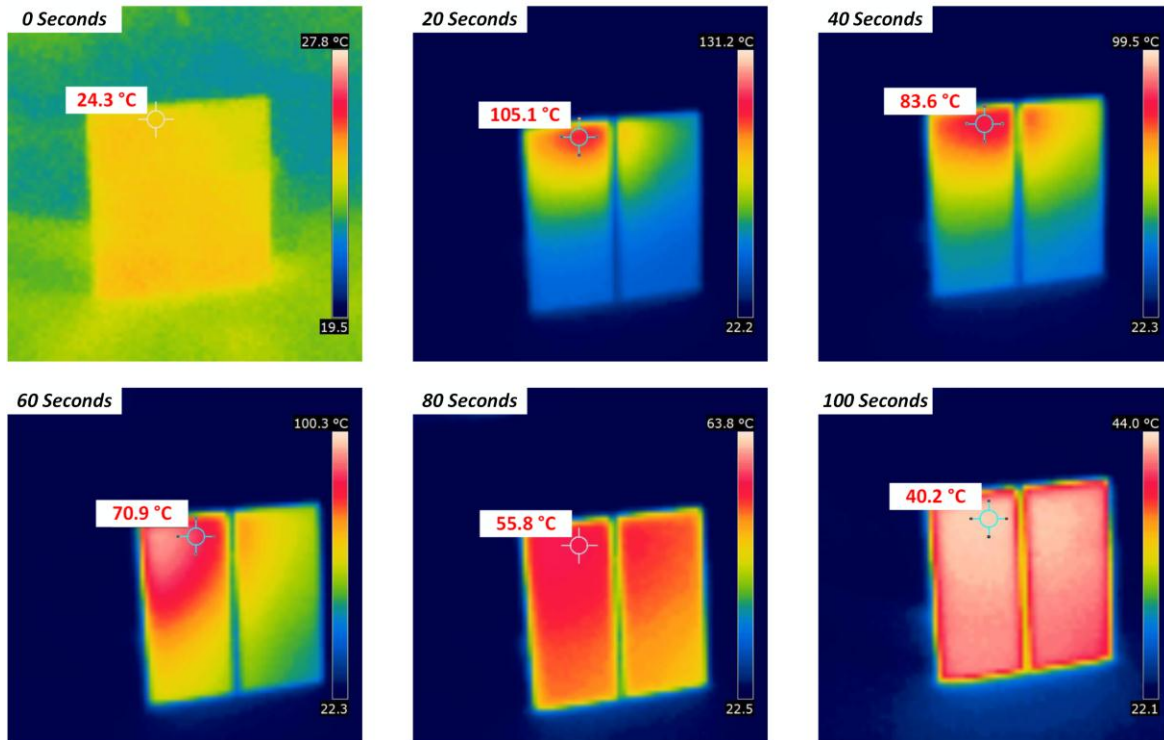

Fig. 11. Heat-Map distribution from 0 to 100 seconds of the cracked solar cell shown in Fig. 9; the solar cell is operated under STC
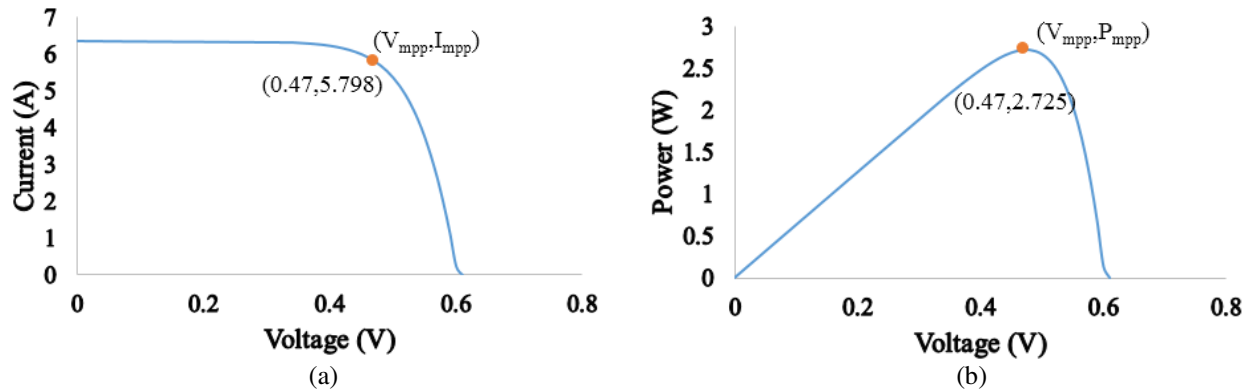
Fig. 12 Obtained I-V & P-V curves of the cracked solar cell sample shown in Fig. 10 under STC

C. Impact of Busbars and Rear Contact Surface Damage due to Micro Cracks and Poor Manufacturing/Soldering Practice

Due to the Another remarkable result was observed while examining the solar cell samples, out of 4000 there are 680 affected by cracks in the busbar. The micro cracks in the busbar leads to significant damage in the metal driving the current from the fingers outer to an external circuit. On the other hand, almost 380 solar cell samples are affected by poor soldiering.

A sample showing a poor adjustment of the busbar metal is shown in Fig. 13. As noticed, there are a number of cracks in the solar wafer, while the busbar contains multiple cracks. The silicon (Si) chemical composition is present instead of original chemical composition of the silver (Ag). This poor busbar structure leads to a second breakdown in the solar cell sample, ultimately causing hot-spot.

The solar cell shown in Fig. 13 has been examined under STC (experimental setup similar to Fig 6). The solar cell has a micro crack as well as poor soldiering in the busbar. It is expected after 10 seconds the heat would increase significantly in the cracked area, and as shown in Fig. 14(a), the temperature of the cracked area increased to abnormal level of 91.4 °C. After 60 seconds, the heat started to expand over the entire solar cell, where the busbar and the cracked area has a temperature of 77.3 °C, as presented in Fig. 14 (b).
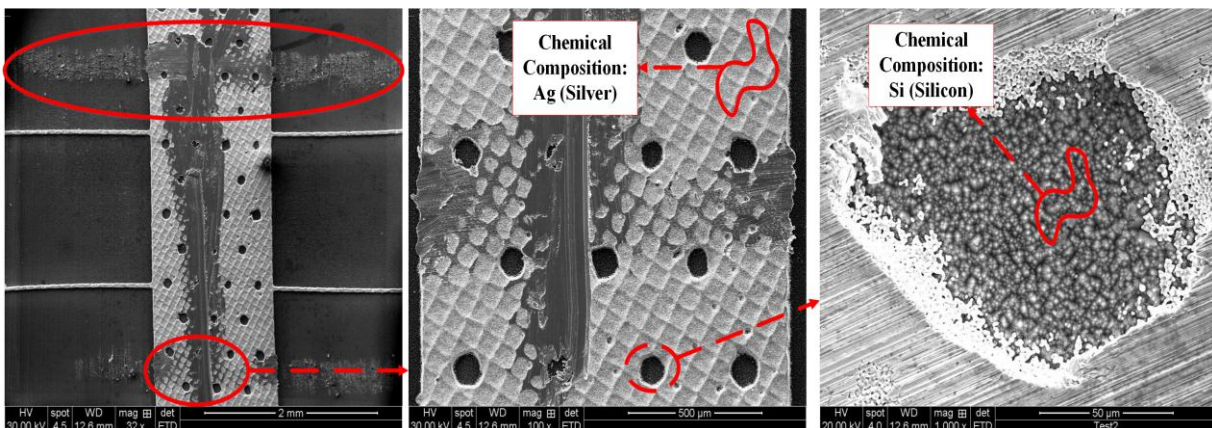

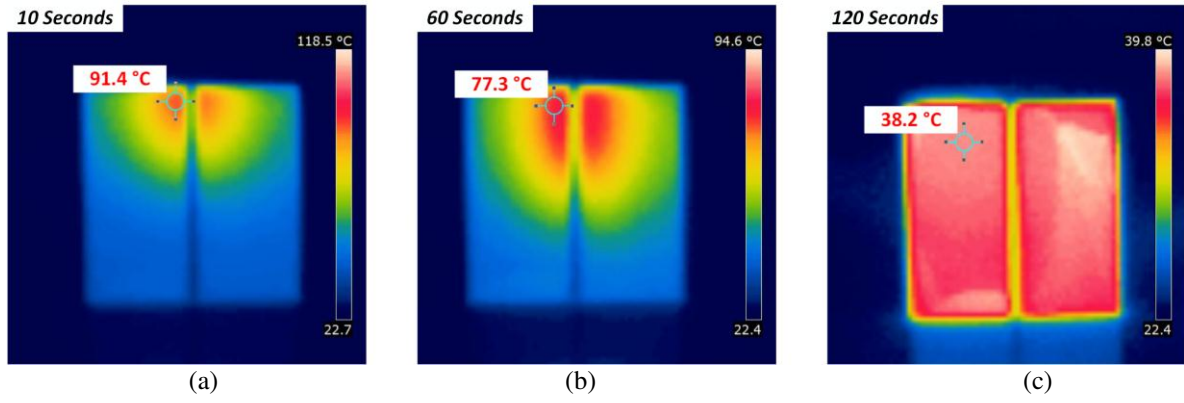Fig. 13. Micro cracks and soldering mismatch in a solar cell busbar

Fig. 14. Heat-Map distribution of the cracked solar cell shown in Fig. 8. (a) After 10 seconds of operating the solar cell under STC, (b) After 60 seconds, (c) After 120 seconds – this level of temperature remains consistent

250 According to Fig. 14(c), the heat is spread all over the solar cell sample, the temperature is equal to 38.2
251 °C; this temperature level stays consistent after 120 seconds. Therefore, this experiment proves that cracks
252 in solar cell busbars have a significant impact on the solar cell heat level, ultimately initiating hot-spots.

253 I-V and P-V curves for the solar cell sample have been measured under STC, results are presented in Fig.
254 15. The measured V_{mpp} of 0.48V is identical with the theoretical predictions (presented earlier in Table 1).
255 However, there is a drop in the maximum output current of 0.15A; I_{mpp} (theoretical: 6.46A) – I_{mpp} (cracked
256 solar cell: 6.31A). Resulting a loss in the output power equals to 2.19%; calculated as follows:

257
$$Power\ Loss\ (\%) = \ 100 - \left(\frac{3.032\ (P_{Micro\ cracked\ solar\ cell})}{3.1\ (P_{Theoretical\ maximum\ power})} \times 100 \right) = \ 2.19\%$$
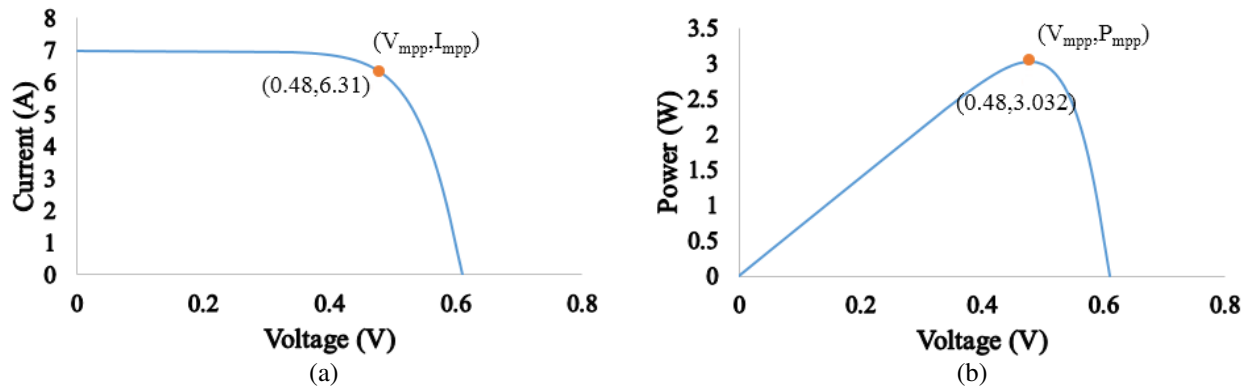

Fig. 15 Obtained I-V & P-V curves of the cracked solar cell sample shown in Fig. 13 under STC

13

258 The rear contact of a typical solar cell is far less important than the front contact, since it is much further
259 away from the junction. However, the design of the rear contact is becoming progressively essential as
260 overall efficiently increases and the solar cells become thinner. During the investigation of the rear contact
261 of the examined solar cells, it was found that 320 solar cells are cracked; 240 samples are cracked in the
262 surface, while 80 samples are cracked in both the surface and the rear busbar. Fig 16 shows the rear
263 contact/view of an examined solar cell sample. The difference between the cracked and non-cracked area
264 are shown in the figure. Principle, the cracked area consists of two chemical composition of aluminum (Al)
265 and silicon (Si), while the non-cracked area is only made of aluminum.

266 As shown in Fig. 16, the non-cracked area has multiple micro cracks of 50 µm width; nevertheless, it does
267 not have a noteworthy loss to the solar cell rear contact. However, the actual size of cracked rear area varies
268 from 4mm to 300 µm. This damage in the rear contact of solar cell resulting a limited open circuit voltage
269 (V_{oc}), subsequently will reduce the efficiency of the cell. In light of what was observed during the
270 experiments, hot-spotting phenomena has no correlation with the presence of micro cracks in solar cells
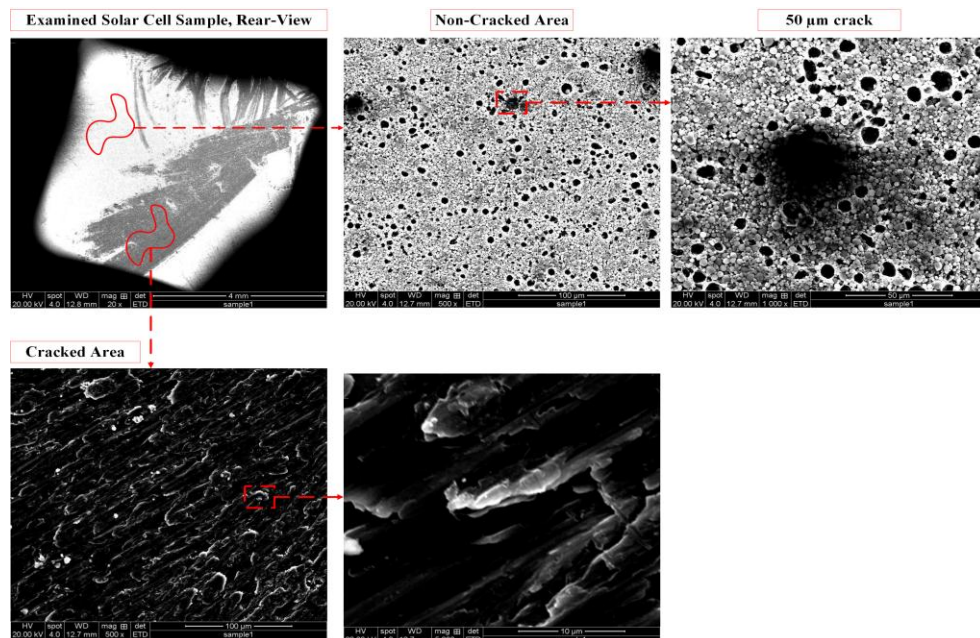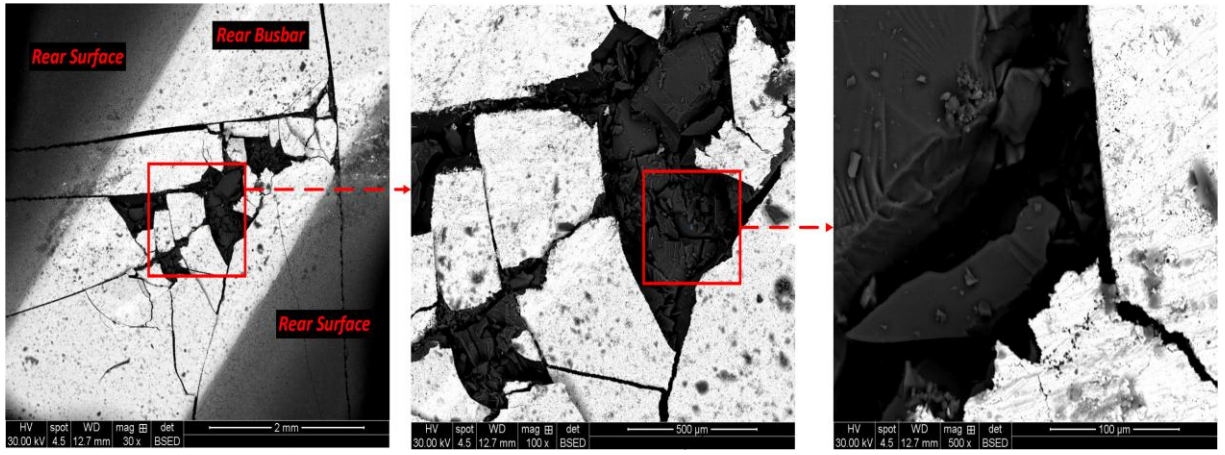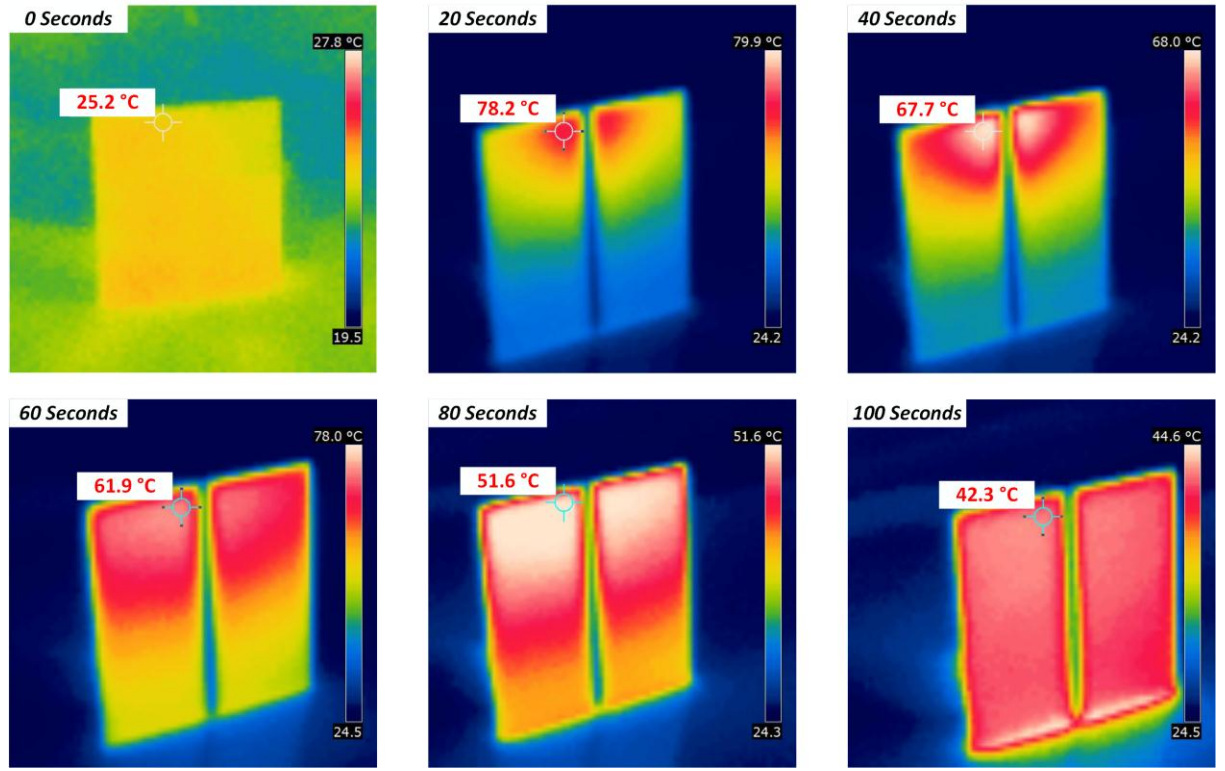271 rear contact surface.

Fig. 16. Micro cracks affecting rear contact of a solar cell

272 Likewise, Fig. 17(a) shows a rear contact image for a solar cell samples affected by micro cracks in the
273 surface and busbar. The solar cell was tested under STC, while the temperature of the cell has been captured
274 and reported in Fig. 17(b); image is taken from 0 seconds to 100 seconds.

275 At zero seconds, the temperature of the cell is equal to 25.2 °C. The temperature of the cracked area raised
276 to 78.2 °C after 20 seconds. Eventually, the heat-level of the cracked area will decrease, due to the expansion
277 of the heat over the cell and would result a temperature levels of 67.7 °C (40 seconds); 61.9 °C (60 seconds);
278 51.6 °C (80 seconds); and 42.3 °C (100 seconds), this level of temperature remains consistent. In light with
279 the results of the heat-distribution, the solar cell had an increase in its temperature of 17.1 °C; final
280 temperature level 42.3 °C – original temperature level 25.2 °C. Therefore, this result shows the impact of
281 micro cracks on the rear contract temperature, while it was evident that there is an abnormal increase in the
282 cell temperature while performing at STC.

(a)

(b)

Fig. 17. Micro cracks affecting rear contact surface and busbar of a solar cell. (a) Crack affected rear surface and busbar; images magnification of 2mm, 500µm and 100µm, (b) Heat-Map distribution from 0 to 100 while the solar cell is illuminated under STC

I-V and P-V curves for the solar cell sample have been measured under STC, results are presented in Fig. 18. The measured V_{mpp} of 0.48V is identical with the theoretical predictions (presented earlier in Table 1). However, there is a drop in the maximum output current of 0.215A; I_{mpp} (theoretical: 6.46A) – I_{mpp} (cracked solar cell: 6.245A). Resulting a loss in the output power equals to 3.29%; calculated as follows:

$$Power\ Loss\ (\%) = 100 - \left(\frac{2.998\ (P_{Micro\ cracked\ solar\ cell})}{3.1\ (P_{Theoretical\ maximum\ power})} \times 100 \right) = 3.29\%$$
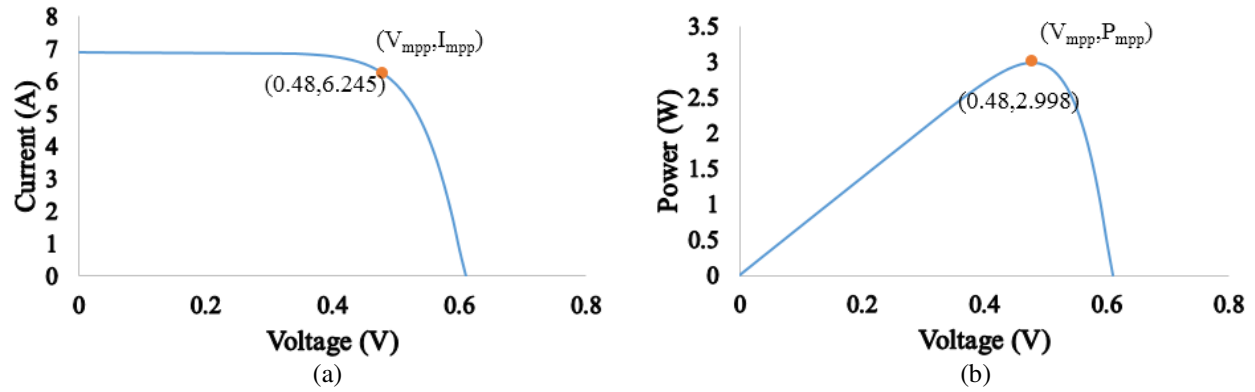
Fig. 18 Obtained I-V & P-V curves of the cracked solar cell sample shown in Fig. 17(a) under STC

IV.   Conclusion

The impact of Photovoltaic (PV) micro cracks has been assessed through the analysis of 4000 polycrystalline silicon solar cells. The inspection of the cracks has been carried out using an electron microscopy, which facilitate the detection of the cracks though the acquisition of both Everhart-Thornley Detector (ETD) and the Back Scatted Electron Diffraction (BSED) image, where it was found that the size micro cracks are ranging from 50µm to a maximum of 4mm. Micro cracks have been categorized into two main categories, including:

1) Front contact cracks affecting wafer, fingers and busbar.
2) Rear contact cracks affecting rear furnace and the busbar.

Various remarkable observations have been found, including:

1) The output power loss due to micro cracks ranging from 0.9 to 42.8%.
2) Cracks in solar cells fingers reduce the finger width, resulting an increase in the power loss by at least 1.7%.
3) There is a significant correlation between PV hot-spots and existence of micro cracks. While the temperature of a cracked solar cell sample could increase by 7.6 °C or more, resulting a permanent hot-spots in the affected cell.

In future, it is intended to investigate the mitigation of micro cracks in solar cells, and develop a novel intelligent detection system to locate and possibly evaluate the impact of such cracks on the output power performance of solar cells.

V.   References

[1]. IEC 61215:2006, International standard, crystalline silicon terrestrial photovoltaic (PV) modules – design qualification and type approval, European committee for Electrotechnical Standardizations. Photovoltaic (PV) module safety qualification.

[2]. Borri, C., Gagliardi, M., & Paggi, M. (2018). Fatigue crack growth in Silicon solar cells and hysteretic behaviour of busbars. Solar Energy Materials and Solar Cells, 181, 21-29.

[3]. Dhimish, M., Holmes, V., Mather, P., Aissa, C., & Sibley, M. (2018). Development of 3D graph-based model to examine photovoltaic micro cracks. Journal of Science: Advanced Materials and Devices, 3(3), 380-388.

[4]. Aly, A., Jensen, S. S., & Pedersen, A. B. (2017). Solar power potential of Tanzania: Identifying CSP and PV hot spots through a GIS multicriteria decision making analysis. Renewable Energy, 113, 159-175.

[5]. Dhimish, M., Holmes, V., Mehrdadi, B., Dales, M., & Mather, P. (2018). Output-power enhancement for hot spotted polycrystalline photovoltaic solar cells. IEEE Transactions on Device and Materials Reliability, 18(1), 37-45.

[6]. Srećković, N., Lukač, N., Žalik, B., & Štumberger, G. (2016). Determining roof surfaces suitable for the installation of PV (photovoltaic) systems, based on LiDAR (Light Detection And Ranging) data, pyranometer measurements, and distribution network configuration. Energy, 96, 404-414.

[7]. Xiang, C., Zhao, X., Tan, L., Ye, J., Wu, S., Zhang, S., & Sun, L. (2019). A solar tube: Efficiently converting sunlight into electricity and heat. Nano Energy, 55, 269-276.

[8]. El-Bashir, S. M., Al-Harbi, F. F., Elburaih, H., Al-Faifi, F., & Yahia, I. S. (2016). Red photoluminescent PMMA nanohybrid films for modifying the spectral distribution of solar radiation inside greenhouses. Renewable Energy, 85, 928-938.

[9]. Bedrich, K. G., Luo, W., Pravettoni, M., Chen, D., Chen, Y., Wang, Z., ... & Wang, Y. (2018). Quantitative Electroluminescence Imaging Analysis for Performance Estimation of PID-Influenced PV Modules. IEEE Journal of Photovoltaics, 8(5), 1281-1288.

[10]. Haase, F., Käsewieter, J., Nabavi, S. R., Jansen, E., Rolfes, R., & Köntges, M. (2018). Fracture Probability, Crack Patterns, and Crack Widths of Multicrystalline Silicon Solar Cells in PV Modules During Mechanical Loading. IEEE Journal of Photovoltaics, 8(6), 1510-1524.

[11]. Dhimish, M., Holmes, V., Dales, M., & Mehrdadi, B. (2017). Effect of micro cracks on photovoltaic output power: case study based on real time long term data measurements. Micro & Nano Letters, 12(10), 803-807.

[12]. Oh, S., Jun, D. H., Shin, K. W., Choi, I., Jung, S. H., Choi, J., ... & Yoon, E. (2016). Control of Crack Formation for the Fabrication of Crack-Free and Self-Isolated High-Efficiency Gallium Arsenide Photovoltaic Cells on Silicon Substrate. IEEE Journal of Photovoltaics, 6(4), 1031-1035.

[13]. Bressan, M., Gutierrez, A., Gutierrez, L. G., & Alonso, C. (2018). Development of a real-time hot-spot prevention using an emulator of partially shaded PV systems. Renewable Energy, 127, 334-343.

[14]. Dhimish, M., Holmes, V., Mather, P., & Sibley, M. (2018). Novel hot spot mitigation technique to enhance photovoltaic solar panels output power performance. Solar Energy Materials and Solar Cells, 179, 72-79.

[15]. Rossi, D., Omaña, M., Giaffreda, D., & Metra, C. (2015). Modeling and detection of hotspot in shaded photovoltaic cells. IEEE Transactions on Very Large Scale Integration (VLSI) Systems, 23(6), 1031-1039.

[16]. Dhimish, M., Mather, P., & Holmes, V. (2018). Evaluating Power Loss and Performance Ratio of Hot-Spotted Photovoltaic Modules. IEEE Transactions on Electron Devices, 65(12), 5419-5427.

[17]. S. Ben-Yaakov, A. Cervera, A. Blumenfeld and M. M. Peretz, "Resonant switched-capacitor gyrator-type converter with local MPPT capability for PV cells". U.S. Patent No. 9,906,189. Washington, DC: U.S. Patent and Trademark Office, Feb. 2018.

357 [18]. Dhimish, M. (2019). Assessing MPPT Techniques on Hot-Spotted and Partially Shaded
358   Photovoltaic Modules: Comprehensive Review Based on Experimental Data. IEEE Transactions
359   on Electron Devices, 66, 1132-1144.
360 [19]. Mao, P., Wei, Y., Li, H., & Wang, J. (2017). Junction diodes in organic solar cells. Nano energy,
361   41, 717-730.
362 [20]. Bressan, M., Gutierrez, A., Gutierrez, L. G., & Alonso, C. (2018). Development of a real-time
363   hot-spot prevention using an emulator of partially shaded PV systems. Renewable Energy, 127,
364   334-343.
365 [21]. Dhimish, M. (2019). 70% decrease of hot-spotted photovoltaic modules output power loss using
366   novel MPPT algorithm. IEEE Transactions on Circuits and Systems II: Express Briefs.
367 [22]. Nolze, G., Winkelmann, A., & Boyle, A. P. (2016). Pattern matching approach to
368   pseudosymmetry problems in electron backscatter diffraction. Ultramicroscopy, 160, 146-154.
369 [23]. Zhang, X., Cen, X., Ravichandran, R., Hughes, L. A., & van Benthem, K. (2016). Simultaneous
370   scanning electron microscope imaging of topographical and chemical contrast using in-lens, in-
371   column, and everhart–thornley detector systems. Microscopy and Microanalysis, 22(3), 565-575.
372 [24]. Bharadwaj, P., Karnataki, K., & John, V. (2018, June). Formation of Hotspots on Healthy PV
373   Modules and Their Effect on Output Performance. In 2018 IEEE 7th World Conference on
374   Photovoltaic Energy Conversion (WCPEC)(A Joint Conference of 45th IEEE PVSC, 28th PVSEC
375   & 34th EU PVSEC) (pp. 0676-0680). IEEE.
376 [25]. Solheim, H. J., Fjær, H. G., Sørheim, E. A., & Foss, S. E. (2013). Measurement and simulation of
377   hot spots in solar cells. Energy Procedia, 38, 183-189.
378 [26]. Geisemeyer, I., Fertig, F., Warta, W., Rein, S., & Schubert, M. C. (2014). Fast Hot Spot
379   Evaluation. 29th EUPVSEC Amsterdam, 2429-2434.